Improved SVD-based Data Compression Method for Synchronous Phasor Measurement in Distribution Networks

Jinli Zhao[a], Yuzhuan Ye[a], Hao Yu[a],*, Peng Li[b], Peng Li[a], Jianzhong Wu[c], Chengshan Wang[a]

[a] Key Laboratory of Smart Grid of Ministry of Education, Tianjin University, Tianjin 300072, China

[b] Digital Grid Research Institute of China Southern Power Grid, Guangzhou, 510670, Guangdong Province, China

[c] Institute of Energy, School of Engineering, Cardiff University, Cardiff CF24 3AA, UK

Abstract: The integration of phasor measurement units (PMUs) greatly improves the operation monitoring level of distribution networks. However, high sampling rates in PMUs generate huge volumes of measurement data, which creates heavy transmission and storage burdens in information and communication systems. In this paper, an improved singular value decomposition (SVD)-based data compression method for PMU measurements in distribution networks is proposed. First, a lossless phase angle conversion method is proposed, which converts the discontinuous phase angle data of PMU into continuous data sequence to enhance the compression performance. Then, a PMU data compression method is proposed based on SVD, and the compression capability is further enhanced by a lossless compression that utilizes the orthogonal property of the two sub-matrices generated by SVD. Moreover, an error control strategy is designed to dynamically optimizes the scale of transmitted data according to the accuracy requirement of different applications in distribution networks. Finally, case studies are performed using real PMU measurement data from a pilot project in China to validate the compression performance and advantages of the proposed method.

Key words: Data compression, Singular value decomposition (SVD), Phasor measurement units (PMUs), Phasor data concentrator (PDC), Distribution network.

---

* Corresponding author. Tel.: +86 137 5218 5093; fax: +86 22 27892810.
E-mail address: tjuyh@tju.edu.cn.

Nomenclature

Abbreviations

SVD	Singular value decomposition
PMU	Phasor measurement unit
WAMS	Wide area measurement system
GPS	Global positioning system
DG	Distributed generator
PDC	Phasor data concentrator
DMS	Distribution management system
PCA	Principal component analysis
DCT	Discrete cosine transform
SCADA	Supervisory control and data acquisition system
EEB	Expected error bound
CR	Compression ratio
RE	Reconstruction error
NMSE	Normalized mean square error
MAE	Maximum absolute error

Indices

i, j	Indices of matrix entries
t	Indices of time periods

Variables

δ, δ'	Increment for phase angle conversion/recovery
$\boxed{\alpha_{i,j}}$	Compressed entries of $\overline{U}_{11}$
s	Number of the retained singular values

$\lambda_{\mathrm{CR}}^{\mathrm{Trad}}$	Compression ratio of traditional method
$\lambda_{\mathrm{CR}}^{\mathrm{Impr}}$	Compression ratio of improved method
$\lambda_{\mathrm{CR}}^{\mathrm{Gain}}$	Gain percentage of compression ratio of improved method
$\varepsilon_{\mathrm{NMSE}}$	Normalized mean square error
$\varepsilon_{\mathrm{MAE}}$	Maximum absolute error

Parameters

Δt	PMU sampling interval
T	Measurement duration time
$\boldsymbol{x}$	PMU measurement column vector
$\boldsymbol{X}, x$	Measurement data matrix and its entry
$\widetilde{\boldsymbol{X}}, \tilde{x}$	Normalized measurement data matrix and its entry
$\widetilde{\boldsymbol{X}}', \tilde{x}'$	Normalized reconstruction data matrix and its entry
$\boldsymbol{X}', x'$	Reconstruction data matrix and its entry
Z^{base}	Base value of the PMU measurement
$\boldsymbol{U}, \boldsymbol{V}^{\mathrm{H}}$	Orthogonal matrices
$\boldsymbol{u}_i, \boldsymbol{v}_i^{\mathrm{H}}$	Left/right singular vectors of normalized measurement data matrix
M, N	Vertical and horizontal dimensions of measurement data matrix
$\boldsymbol{\Sigma}, \boldsymbol{\Sigma}'$	Diagonal matrix
$\boldsymbol{U}_{11}, \boldsymbol{U}_{12}, \boldsymbol{U}_{21}, \boldsymbol{U}_{22}$	Sub-matrices of orthogonal matrix $\boldsymbol{U}$
$\boldsymbol{V}_{11}^{\mathrm{H}}, \boldsymbol{V}_{12}^{\mathrm{H}}, \boldsymbol{V}_{21}^{\mathrm{H}}, \boldsymbol{V}_{22}^{\mathrm{H}}$	Sub-matrices of orthogonal matrix $\boldsymbol{V}^{\mathrm{H}}$
$\overline{\boldsymbol{U}}_{11}, \overline{\boldsymbol{V}}_{11}^{\mathrm{H}}$	Compressed sub-matrices
s^{max}	Maximum number of the retained singular values
$\varepsilon^{\mathrm{Exp}}$	Expected error bound

1. Introduction

In recent years, due to the increasing penetration of intermittent distributed generators (DGs) [1] [2], the dynamics of power distribution networks have become more and more complex and uncertain [3], which creates challenges for system monitoring and operation, and places a higher requirement on advanced metering and sensor technologies [4]. Fast and accurate measurements provided by phasor measurement units (PMUs) can significantly improve the monitoring level, system observability, and flexibility of distribution networks [5]. Synchronized by global positioning system (GPS), PMU can provide high-precision time stamp data frames that contain the phasors of voltage and current, system frequency, and corresponding rates of change, as well as active/reactive powers at the given sampling rate [6] [7]. For a distribution network equipped with small-scale PMUs, the PMU data can be directly transmitted to a distribution management system (DMS) [8] through fiber or wireless communication. As increasing number of PMUs are installed in distribution networks, there is a need to deploy phasor data concentrators (PDCs) to gather measurements from multiple PMUs and send them to the DMS so as to alleviate the burden on communication systems.

Although the use of high-precision synchronous phasor measurements helps system operators to understand the dynamic behaviors of distribution networks, PMUs also generate a large volume of data due to their high sampling rates (30~100Hz) [9] [10]. As a result, communication networks have to bear heavy burdens of information transmission and processing. Sometimes, this may cause unacceptable latency and serious congestion in communication networks. Moreover, the existing communication infrastructure of distribution networks cannot completely satisfy the requirements of real-time PMU data communication in terms of coverage, scalability, and bandwidth demand [11]. Network bandwidth demand increases linearly with the number of installed PMUs. Hence, it is of great importance that PMU data be compressed to alleviate

communication bandwidth demands.

The operation of distribution networks places diverse demands on PMU data [12], including fault detection and location [13], state estimation [14] [15], optimal voltage control [16], and power supply restoration [17]. These goals require different performances for PMU measurements, such as data accuracy, response speed and real-time performance. Real-time PMU measurements are needed to satisfy time-critical applications, e.g. pilot protection and fault location [18]. On the other hand, as one of the core components of DMS, distribution system state estimation can convert redundant meter readings and other pseudo measurements into an estimate of the state so as to provide accurate data for monitoring and analyses [19] [20]. The existing state estimation of distribution networks typically have refresh rates at 15 minutes [21]. Voltage regulation based on power electronic devices may change every ten to one hundred seconds [22].

Considering the different demands in distribution networks, data compression is regarded as an effective way to mitigate the burden of communication networks. Data compression methods can mainly be divided into two categories [23]: lossless and lossy compression. With the former, the original data can be completely restored, whereas with lossy compression, the original data will suffer some information loss [24]. Lossy compression has attracted more attention due to its potential to achieve higher compression ratios (CRs) than can be achieved by lossless methods. Ref. [25] shows that lossless compression directly applied to signal data might reach CRs ranging from 2 to 5, while lossy compression can obtain higher CRs due to the loss of information integrity.

Many studies have been conducted for the data compression of PMU [24] [25]. Ref. [26] presented an unequal-interval reduction method to reduce the scale of PMUs' data in substations of WAMS. In [27], an SVD-based compression method was used to compress the data from supervisory control and data acquisition system (SCADA). In [28], a compressive sampling theory was

used to reduce the network bandwidth requirements of WAMS. Ref. [29] proposed a method to compress the archived PMU data of WAMS. It combines the principal component analysis (PCA) and discrete cosine transform (DCT), and thus to eliminate the spatial and temporal redundancies in the WAMS data recorded by multiple PMUs to reduce the physical memory requirements. These methods can also be applied to the compression of phase angle data of PMU. The neglect of the discontinuities of PMU phase angle data lowers the compression ratio. Some efforts have been made to address the problem. For example, ref. [30] proposed a real-time data compression technique for PMU data, in which the compression result of the amplitude data of voltage or current is used to determine whether the corresponding phase date should be retained. This method ignores the internal dynamics of phase angle data and the reconstruction error may be increased. Besides, the diverse applications in distribution networks pose different demands on PMU data, especially on data accuracy and time delay. Therefore, the compression method should be able to adjust the compression ratio and accuracy to flexibly satisfy the need of different applications in distribution networks.

An improved SVD-based compression method for PMU data is proposed in this paper. Our work aims to develop a data compression method for the PDC that integrates multiple PMUs, in order to alleviate the communication burden from PDC to DMS. The PMU data are time-tagged and continuously transmitted to the receiving terminals of DMS after compression. The reconstructed data can adequately satisfy the accuracy and timeliness requirement of the typical applications in distribution networks such as state estimation and energy management. The main contributions are summarized as follows:

1) A lossless phase angle conversion method is proposed to enhance the compression performance of phase angle data of PMU. The method can eliminate the discontinuities in phase angle data due to the bounded range of PMU and restore the original data exactly, thus providing a

favorable precondition for data compression.

2) An improved SVD-based compression method for PMU is proposed. Lossless compression is performed on the basis of SVD method to achieve a higher CR. An error control strategy is designed for the dynamic CR adjustment. The scale of transmitted data can be effectively optimized under a given error constraint by regulating the number of retained singular values.

The remainder of this paper is organized as follows. In Section 2, the construction of PMU measurement data matrix and data pre-processing are proposed. The data compression based on SVD is proposed in Section 3. Section 4 presents the dynamic optimization strategy for maximizing data compression while maintaining data accuracy. Case studies are given in Section 5 to validate the effectiveness of the proposed method using real PMU measurement data. Finally, conclusions are drawn in Section 6.

2. Data pre-processing and singular value decomposition

2.1. Construction of PMU measurement data matrix and data pre-processing

1) Preparation of PMU measurement data matrix

Data collected by PDC from multiple PMUs can be naturally represented by a large measurement data matrix. Assume that there are same type measurements from M different PMUs, e.g. nodal voltage amplitude, branch current amplitude, voltage or current phase angle, active power or reactive power, and system frequency. At the sampling time t, the same type measured data are formed as a column vector $\boldsymbol{x}(t) = \left[x_{1,t}, x_{2,t}, \cdots, x_{M,t}\right]^{\mathrm{T}}$. Suppose that PMUs have the same sampling interval Δt and measurement duration time T; hence a PMU will generate $N = \frac{T}{\Delta t} + 1$ sampling data. As a result, a measurement data matrix $\boldsymbol{X} = [\boldsymbol{x}(1), \cdots \boldsymbol{x}(t), \cdots, \boldsymbol{x}(N)] \in \mathbb{C}^{M \times N}$ is obtained by arranging the column vectors $\boldsymbol{x}(t)$ in chronological order.

2) Conversion and recovery of phase angle data

According to IEEE Std. C37.118.1 [33], the phase angle of measured voltage or current fluctuates from $-\pi$ to π, which is highly related to the system frequency, as expressed in Eq. (1).

$$\varphi(t) = 2\pi f_0 t + \left[2\pi \int (f(t) - f_0)\, dt + \phi \right] \tag{1}$$

where f_0 is the nominal frequency, and ϕ is the instantaneous phase angle relative to a cosine function at the nominal frequency. Fig. 1 shows the relationship between phase angle and system frequency. When system frequency is higher than the nominal frequency (50Hz), phase angle increases due to the integration of frequency. A similar situation occurs when the frequency is lower than the nominal frequency. In this case, phase angle will decrease.
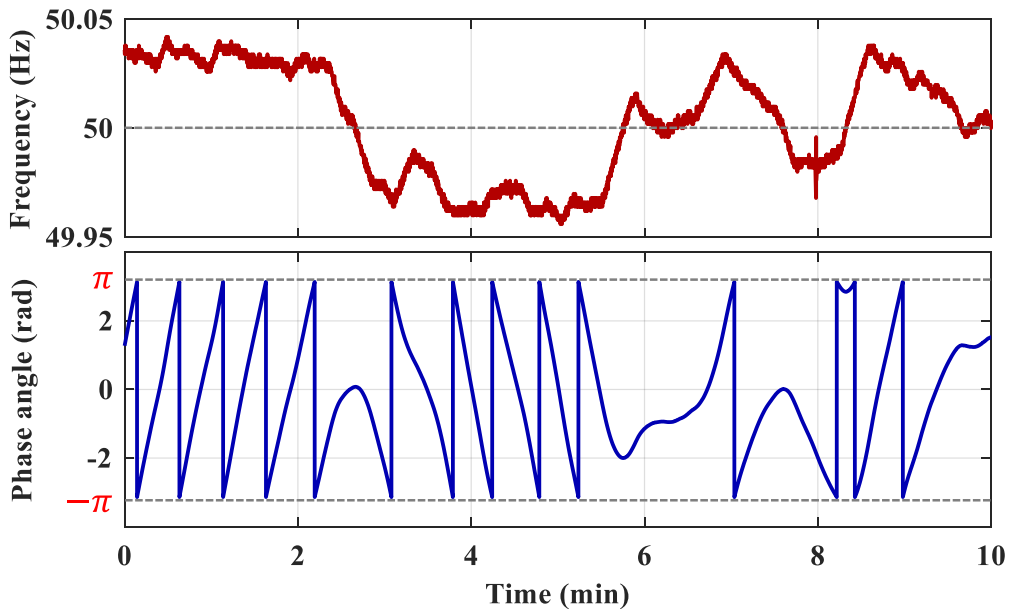

Fig. 1. Relationship between phase angle and system frequency.

The range of phase angle of PMU is $[-\pi, \pi)$. This means that the value of phase angle will experience a sudden change when crossing the boundaries of $-\pi$ and π. The discontinuity occurs frequently in the actual operation of distribution networks and may lower the compression performance of phase angle. To enhance the compression performance, a phase angle conversion method is proposed to convert the original phase angle data into a continuous data sequence, as

shown in Eqs. (2) and (3). Each row of the matrix is converted separately, and the first element of each row remains the same. That is, the conversion starts with the second element.

$$x_{i,j}^{con} = \begin{cases} x_{i,j} + \delta_{i,j}, & x_{i,j} < x_{i,j-1}^{con} \\ x_{i,j} - \delta_{i,j}, & x_{i,j} \geq x_{i,j-1}^{con} \end{cases} \tag{2}$$

$$\delta_{i,j} = \left\lfloor \frac{\left| x_{i,j} - x_{i,j-1}^{con} \right| + \pi}{2\pi} \right\rfloor \times 2\pi \tag{3}$$

where $x_{i,j}^{con}$ denotes the phase angle after being converted. $\delta_{i,j}$ represents the increment required for phase angle conversion, and $\lfloor \cdot \rfloor$ represents that " $\cdot$ " is rounded down to the nearest integer. In particular, increment $\delta_{i,j}$ can only be a non-negative integer multiple of 2π.

The derived data sequence can be restored to the original phase angle data equivalently. Eq. (3) guarantees increment $\delta_{i,j}$ is a non-negative integer multiple of 2π. Therefore, in the recovery stage, all the data points located outside of $[-\pi, \pi)$ are moved back to the original interval with a bias of integer multiples of 2π. The recovery process is given as follows.

$$x_{i,j}^{rec} = \begin{cases} x_{i,j}^{con}, & -\pi \leq x_{i,j}^{con} < \pi \\ x_{i,j}^{con} - \delta_{i,j}', & x_{i,j}^{con} = k\pi \\ x_{i,j}^{con} - \delta_{i,j}'', & x_{i,j}^{con} > \pi \text{ and } x_{i,j}^{con} \neq k\pi \\ x_{i,j}^{con} + \delta_{i,j}''', & x_{i,j}^{con} < -\pi \end{cases} \tag{4}$$

$$\begin{cases} \delta_{i,j}' = (k+1) \times \pi, & x_{i,j}^{con} = k\pi \\ \delta_{i,j}'' = \left\lceil \frac{x_{i,j}^{con} - \pi}{2\pi} \right\rceil \times 2\pi, & x_{i,j}^{con} > \pi \text{ and } x_{i,j}^{con} \neq k\pi \\ \delta_{i,j}''' = \left\lceil \frac{-\left(x_{i,j}^{con} + \pi\right)}{2\pi} \right\rceil \times 2\pi, & x_{i,j}^{con} < -\pi \end{cases} \tag{5}$$

where $k \in \{1, 3, 5, \cdots\}$, $x_{i,j}^{rec}$ denotes the phase angle data after being recovered, and $\delta_{i,j}'$, $\delta_{i,j}''$ and $\delta_{i,j}'''$ represent the increment required for phase angle recovery. And $\lceil \cdot \rceil$ represents that " $\cdot$ " is rounded up to the nearest integer. The increment $\delta_{i,j}'$, $\delta_{i,j}''$ and $\delta_{i,j}'''$ can only be a positive integer multiple of 2π.

The conversion and recovery method for the phase angle is lossless, that is, $x_{i,j}^{\text{rec}} \equiv x_{i,j}$. A theoretical proof is presented in Appendix A. Fig. 2 shows the voltage phase angle curve to validate the effectiveness of the proposed method. It is shown that the original discontinuous phase angles are converted into continuous data sequence. The continuous data sequence can also be completely restored as the original data without any loss of phase angle information.
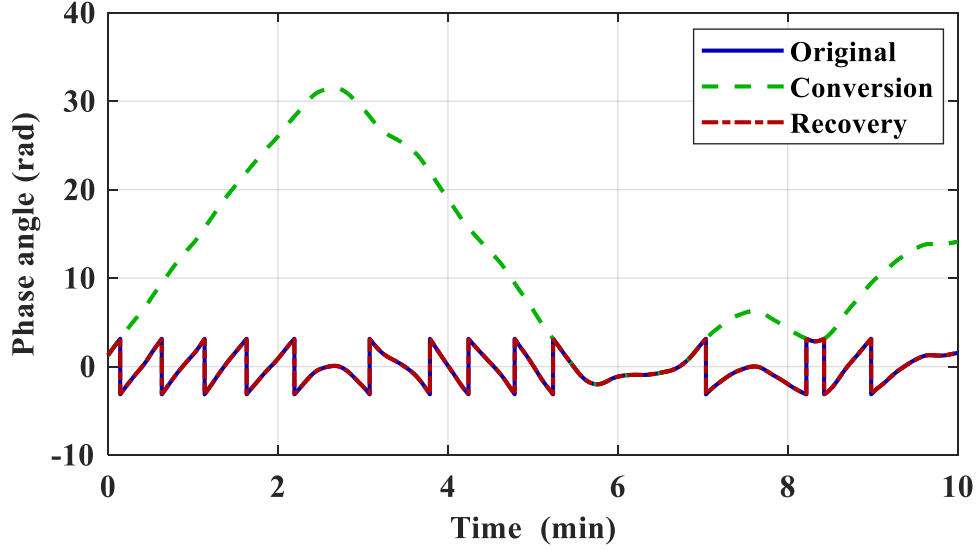

Fig. 2. Data conversion and recovery of voltage phase angle.

3) Normalization processing

The measurements from multiple PMUs usually have different magnitudes, especially for current and active/reactive power. The difference in the order of magnitude among the data in matrix X may weaken the accuracy of SVD. Therefore, to improve the efficiency and accuracy of SVD, matrix X is converted into a normalized measurement data matrix $\widetilde{X} \in \mathbb{C}^{M \times N}$, as expressed in Eq. (6).

$$\tilde{x}_{i,j} = \frac{x_{i,j}}{Z^{\text{base}}} \tag{6}$$

where Z^{base} denotes the base value of the PMU measurement, and it can be the rated value of the PMU data.

2.2. Singular value decomposition for normalized measurement matrix

The SVD technique can be directly used to decompose the normalized measurement data matrix $\widetilde{X}$ into a product of three matrices [27], as expressed in Eq. (7).

$$\widetilde{X} = U\Sigma V^{\mathrm{H}} \tag{7}$$

In Eq. (7), $U = (u_1, \cdots, u_M) \in \mathbb{C}^{M \times M}$ and $V^{\mathrm{H}} = (v_1^{\mathrm{H}}, \cdots, v_N^{\mathrm{H}})^{\mathrm{T}} \in \mathbb{C}^{N \times N}$ are orthogonal matrices containing eigenvectors of $\widetilde{X}\widetilde{X}^{\mathrm{T}}$ and $\widetilde{X}^{\mathrm{T}}\widetilde{X}$, respectively. And $\Sigma \in \mathbb{C}^{M \times N}$ is a diagonal matrix whose elements are the singular values, which are the square roots of the eigenvalues of $\widetilde{X}\widetilde{X}^{\mathrm{T}}$ sorted in descent. Superscripts T and H denote the transposition and conjugate transposition of the matrix, respectively.

The merit of the SVD method is that the sorted singular values decrease rapidly, which means that most of the status information is packed in the high-value singular values, while the low-value singular values mainly represent the noise. This property allows for the low-error approximation of the original matrix by retaining only a few high-value singular values. Fig. 3 illustrates the reduction and accumulation percentage of the sorted singular values of the voltage normalized measurement data matrix. The measurement data matrix consists of voltage amplitude data of 13 PMUs arranged in sequence. It can be seen that the sorted singular values in diagonal matrix Σ decrease rapidly then decrease slowly, which is the main motivation for employing SVD to PMUs data compression.
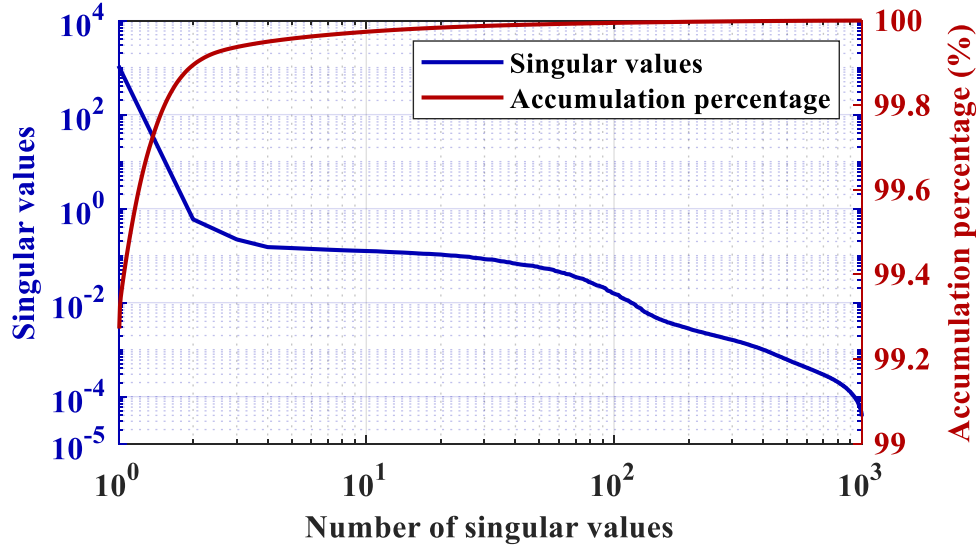
Fig. 3. Reduction and accumulation percentage of the sorted singular values.

3. Data compression based on SVD and data reconstruction

3.1. SVD based data compression

SVD offers low rank approximations by selecting only the high-value singular values that contain most of the status information of the compressed matrix. Suppose that s singular values are selected from $\boldsymbol{\Sigma}$ to form a new diagonal matrix $\boldsymbol{\Sigma}'$, which contains the retained singular values for data reconstruction, as shown in Eq. (8).

$$\boldsymbol{\Sigma}' = \begin{bmatrix} \boldsymbol{\Sigma}_{11}^{',s\times s} & \boldsymbol{0}^{s\times(N-s)} \\ \boldsymbol{0}^{(M-s)\times s} & \boldsymbol{0}^{(M-s)\times(N-s)} \end{bmatrix} \tag{8}$$

After s singular values are determined, the orthogonal matrices $\boldsymbol{U}$ and $\boldsymbol{V}^{\mathrm{H}}$ can be divided into four sub-matrices respectively, as shown in Eqs. (9) and (10).

$$\boldsymbol{U} = \begin{bmatrix} \boldsymbol{U}_{11}^{s\times s} & \boldsymbol{U}_{12}^{s\times(M-s)} \\ \boldsymbol{U}_{21}^{(M-s)\times s} & \boldsymbol{U}_{22}^{(M-s)\times(M-s)} \end{bmatrix} \tag{9}$$

$$\boldsymbol{V}^{\mathrm{H}} = \begin{bmatrix} \boldsymbol{V}_{11}^{\mathrm{H},s\times s} & \boldsymbol{V}_{12}^{\mathrm{H},s\times(N-s)} \\ \boldsymbol{V}_{21}^{\mathrm{H},(N-s)\times s} & \boldsymbol{V}_{22}^{\mathrm{H},(N-s)\times(N-s)} \end{bmatrix} \tag{10}$$

For the traditional SVD-based data compression, only $\boldsymbol{U}_{11}^{s\times s}$, $\boldsymbol{U}_{21}^{(M-s)\times s}$, $\boldsymbol{\Sigma}_{11}^{',s\times s}$, $\boldsymbol{V}_{11}^{\mathrm{H},s\times s}$ and $\boldsymbol{V}_{12}^{\mathrm{H},s\times(N-s)}$ are needed to calculate the normalized reconstruction data matrix $\widetilde{\boldsymbol{X}}'$. According to

the dimension information, the total number of elements to be stored after compression is $(M + N + 1) \times s$, which is far less than the original data scale $M \times N$.

In fact, considering that the eigenvectors in orthogonal matrices $\boldsymbol{U}$ and $\boldsymbol{V}^{\mathrm{H}}$ are orthogonal and unitary, there is no need to transmit or store all the elements of the eigenvectors. For sub-matrix $\boldsymbol{U}_{11}$, if the elements in the first column are preserved, all the upper triangular elements above the diagonal can be further compressed. Similar process is also effective for the sub-matrix $\boldsymbol{V}_{11}^{\mathrm{H}}$. That is, only the elements in the first row are preserved, while all the lower triangular elements below the diagonal can be further compressed. For simplification, sub-matrices $\boldsymbol{U}_{11}$ and $\boldsymbol{V}_{11}^{\mathrm{H}}$ are called sub-matrices $\overline{\boldsymbol{U}}_{11}$ and $\overline{\boldsymbol{V}}_{11}^{\mathrm{H}}$ after being compressed, respectively.

The improved SVD-based PMUs data compression is schematically shown in Fig. 4. The SVD-based compression is lossy, due to some low-value singular values being neglected during the compression process. The further compression to $\overline{\boldsymbol{U}}_{11}$ and $\overline{\boldsymbol{V}}_{11}^{\mathrm{H}}$ is lossless because of the utilization of orthogonal property.
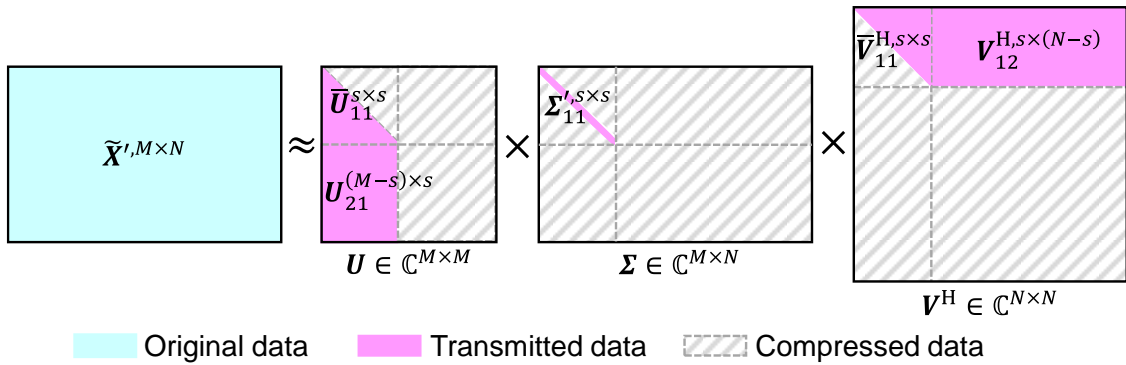

Fig. 4. Schematic of improved SVD-based PMU data compression.

3.2. Data reconstruction

Since the column vectors in the matrix $\boldsymbol{U}$ are orthogonal to each other, i.e., $\boldsymbol{u}_1 \cdot \boldsymbol{u}_2 = 0$, $\boldsymbol{u}_1 \cdot \boldsymbol{u}_3 = 0$, $\boldsymbol{u}_2 \cdot \boldsymbol{u}_3 = 0, \cdots$, where $\boldsymbol{u}_i$ are column vectors of the matrix $\boldsymbol{U}$, the compressed elements of $\overline{\boldsymbol{U}}_{11}$ can be easily recovered by solving a set of linear equations, thus formed in Eq. (11).

$$
\begin{array}{ll}
① & \left\{ u_{1,1}\boxed{\alpha_{1,2}} + u_{2,1}u_{2,2} + u_{3,1}u_{3,2} + \cdots + u_{M-1,1}u_{M-1,2} + u_{M,1}u_{M,2} = 0 \right. \\[4pt]
② & \left\{ \begin{array}{l} u_{1,1}\boxed{\alpha_{1,3}} + u_{2,1}\boxed{\alpha_{2,3}} + u_{3,1}u_{3,3} + \cdots + u_{M-1,1}u_{M-1,3} + u_{M,1}u_{M,3} = 0 \\ \alpha_{1,2}\boxed{\alpha_{1,3}} + u_{2,2}\boxed{\alpha_{2,3}} + u_{3,2}u_{3,3} + \cdots + u_{M-1,2}u_{M-1,3} + u_{M,2}u_{M,3} = 0 \end{array} \right. \\[8pt]
\vdots\quad\vdots & \\[4pt]
ⓢ\text{-①} & \left\{ \begin{array}{l} u_{1,1}\boxed{\alpha_{1,s}} + u_{2,1}\boxed{\alpha_{2,s}} + u_{3,1}\boxed{\alpha_{3,s}} + \cdots + u_{M-1,1}u_{M-1,s} + u_{M,1}u_{M,s} = 0 \\ \alpha_{1,2}\boxed{\alpha_{1,s}} + u_{2,2}\boxed{\alpha_{2,s}} + u_{3,2}\boxed{\alpha_{3,s}} + \cdots + u_{M-1,2}u_{M-1,s} + u_{M,2}u_{M,s} = 0 \\ \qquad\qquad\qquad\qquad\qquad\vdots \\ \alpha_{1,s-1}\boxed{\alpha_{1,s}} + \alpha_{2,s-1}\boxed{\alpha_{2,s}} + \alpha_{3,s-1}\boxed{\alpha_{3,s}} + \cdots + u_{M-1,s-1}u_{M-1,s} + u_{M,s-1}u_{M,s} = 0 \end{array} \right.
\end{array}
\tag{11}
$$

The above equation sets are solved sequentially in $s-1$ steps, where the unknown elements to be solved in each step are the compressed elements in sub-matrices $\overline{U}_{11}$, denoted in boxed notation as $\boxed{\alpha_{i,j}}$ in Eq. (11). Specifically, we can solve the first equation set to obtain unknown $\boxed{\alpha_{1,2}}$, then substitute it into the second equation set to solve unknowns $\boxed{\alpha_{1,3}}$ and $\boxed{\alpha_{2,3}}$. These solutions are further substituted into the third equations, and so on. There are one, two, three, all the way up to $s-1$ unknown elements in the linear equation sets in each step, respectively. The solutions are continuously substituted into the next equations to solve the unknowns. Finally recover all the compressed elements.

Similar process can be performed to the orthogonal matrix V^{H} so as to recover the compressed elements in sub-matrix $\overline{V}_{11}^{\mathrm{H}}$. It should be mentioned that the row vectors of V^{H} are orthogonal to each other, i.e., the linear equations are established based on row vectors v^{H}.

After the compressed elements in sub-matrices $\overline{U}_{11}$ and $\overline{V}_{11}^{\mathrm{H}}$ are recovered, the normalized reconstruction data matrix $\widetilde{X}'$ can be calculated by replacing Σ with Σ', as expressed in Eq. (12).

$$
\widetilde{X}' = U\Sigma'_{11}V^{\mathrm{H}} = \begin{bmatrix} \overline{U}_{11}\Sigma'_{11}\overline{V}_{11}^{\mathrm{H}} & \overline{U}_{11}\Sigma'_{11}V_{12}^{\mathrm{H}} \\ U_{21}\Sigma'_{11}\overline{V}_{11}^{\mathrm{H}} & U_{21}\Sigma'_{11}V_{12}^{\mathrm{H}} \end{bmatrix}
\tag{12}
$$

Considering that the number of compressed data for each sub-matrix $\overline{U}_{11}$ and $\overline{V}_{11}^{\mathrm{H}}$ is $\frac{s\times(s-1)}{2}$, thus, the total number of compressed data is $s \times (s-1)$. Therefore, the amount of data to be maintained and transmitted to DMS is $(M + N - s + 2) \times s$, which is also less than the amount of data to be maintained and transmitted when using the traditional compression method.

Before analysing and applying the PMUs' data, it is necessary to restore the normalized value to its actual value. That is, converting matrix $\widetilde{X}'$ into a reconstruction data matrix $X' \in \mathbb{C}^{M \times N}$ with the following equation.

$$x'_{i,j} = \tilde{x}'_{i,j} \times Z^{\text{base}} \tag{13}$$

3.3. Evaluation of the compression method

Compression performance (i.e. compression ratio) and accuracy of the reconstructed data (i.e. reconstruction error) are usually used to evaluate data compression methods.

1) Compression ratio (CR)

CR has been illustrated in several ways in the literature [27] [30]. For instance, when the storage space of a single compressed data is the same as the original data, CR can be defined as the ratio of raw data size over the sent data size. For the traditional SVD-based method, since the total number of maintained data is $(M + N + 1) \times s$, the CR can be described by Eq. (14). For the improved SVD-based method, $\frac{s \times (s-1)}{2}$ data of sub-matrices $\overline{U}_{11}$ and $\overline{V}_{11}^{\text{H}}$ have been further compressed. The new CR can be derived as Eq. (15). Then, the CR gain percentage of the improved compression method can be easily calculated as Eq. (16).

$$\lambda_{\text{CR}}^{\text{Trad}} = \frac{M \times N}{(M + N + 1) \times s} \tag{14}$$

$$\lambda_{\text{CR}}^{\text{Impr}} = \frac{M \times N}{(M + N - s + 2) \times s} \tag{15}$$

$$\lambda_{\text{CR}}^{\text{Gain}} = \frac{\lambda_{\text{CR}}^{\text{Impr}} - \lambda_{\text{CR}}^{\text{Trad}}}{\lambda_{\text{CR}}^{\text{Trad}}} \times 100\% = \frac{(s - 1)}{(M + N - s + 2)} \times 100\% \tag{16}$$

2) Reconstruction error (RE)

The difference between the raw data and the reconstructed data is defined as RE. In this paper, the normalized mean square error (NMSE) $\varepsilon_{\text{NMSE}}$ [31] and maximum absolute error (MAE) ε_{MAE} [32] are used to describe the RE, as can be seen in Eq. (17).

$$\begin{cases} \varepsilon_{\mathrm{NMSE}}(i) = \dfrac{\sum_{j=1}^{N}\left|x_{i,j}-x_{i,j}'\right|^2}{\sum_{j=1}^{N}\left|x_{i,j}\right|^2} & (i=1,2,\cdots,M) \\ \varepsilon_{\mathrm{MAE}}(i) = \max_{1\le j\le N}\left|x_{i,j}-x_{i,j}'\right| \end{cases} \qquad (17)$$

In Eq. (17), $\varepsilon_{\mathrm{NMSE}}(i)$ is a dimensionless scalar that reflects the average of the sum of deviations between the original data and reconstructed data; $\varepsilon_{\mathrm{MAE}}(i)$ defines the maximum absolute deviation between the original data and reconstructed data.
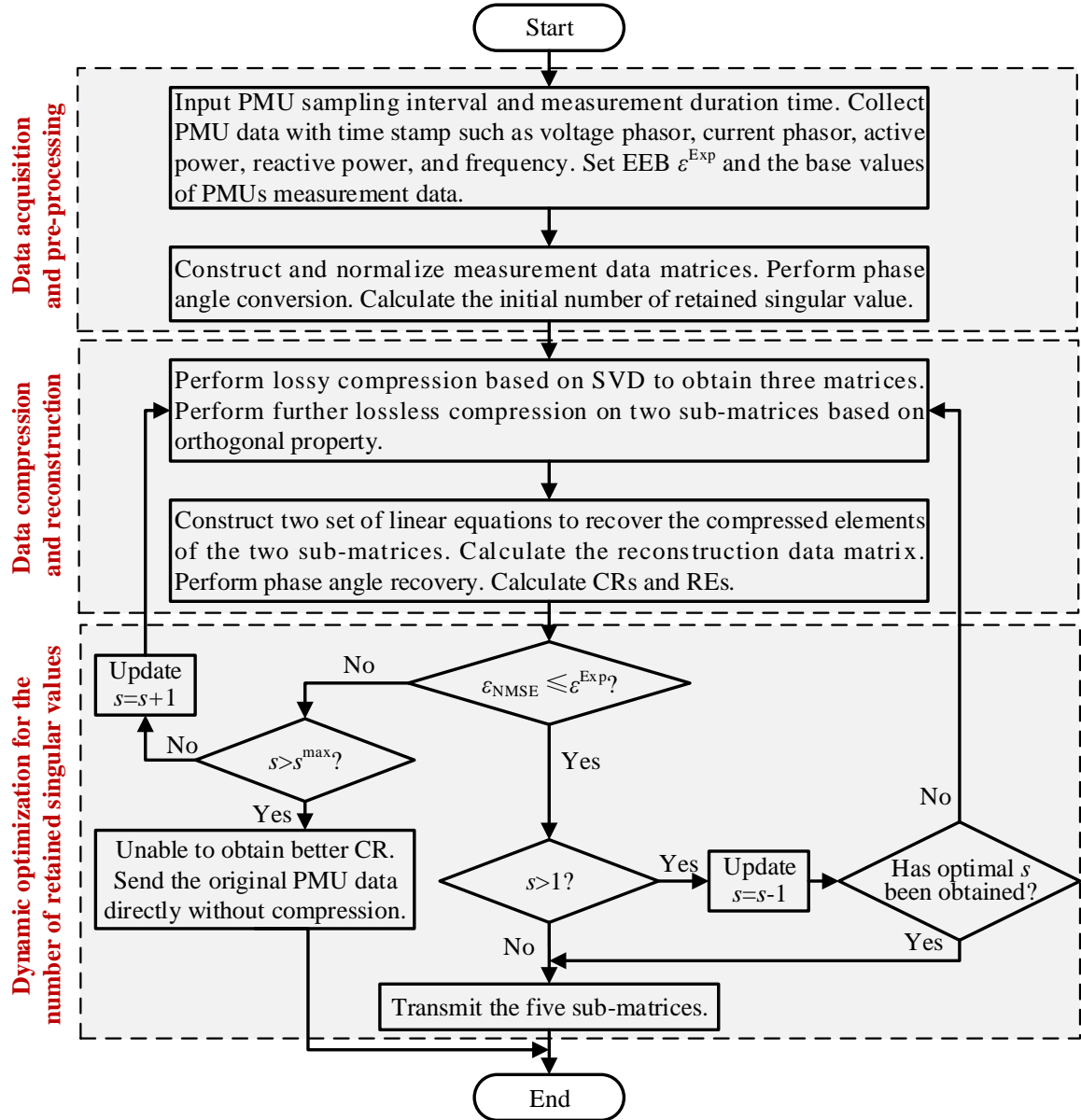

Fig. 5. Flow chart of the improved SVD-based PMU data compression.

4. Dynamic optimization for the number of retained singular values

In this section, an error control strategy is designed for the dynamic CR adjustment. The scale of transmitted data can be effectively optimized under an expected error bound (EEB) by regulating the number of retained singular values. With the optimal number of retained singular values, CR can be maximized while satisfying the accuracy requirement of PMU applications. The corresponding flow chart is shown in Fig. 5.

4.1. Initialization of the number of retained singular values

For effective data compression, CR should be larger than 1, that is $\lambda_{\mathrm{CR}}^{\mathrm{Impr}} > 1$, as expressed in Eq. (18). Then a quadratic inequality is further obtained in Eq. (19). Solving the inequality, we can obtain the maximum permissible number of retained singular values for data compression, as described in Eq. (20).

$$\lambda_{\mathrm{CR}}^{\mathrm{Impr}} = \frac{M \times N}{(M + N - s + 2) \times s} > 1 \tag{18}$$

$$s^2 - (M + N + 2) \times s + M \times N > 0 \tag{19}$$

$$s < s^{\max} = \frac{(M + N + 2) - \sqrt{(M + N + 2)^2 - 4 \times M \times N}}{2} \tag{20}$$

The distribution of singular values provides information to estimate the changing trend of reconstruction error. On this basis, an estimation method is designed for the initial number of retained singular values. The sequence number of the point that has the longest distance to the line between the start and end singular values is assigned as the initial number of retained singular values s_0, as shown in Eqs. (21) and (22).

$$s_0 = \arg \max_{k \in \Omega} d_k \tag{21}$$

$$d_k = \frac{\left| \frac{\sigma_{s^m} - \sigma_1}{s^m - 1} \times (k - 1) - \sigma_k + \sigma_1 \right|}{\sqrt{1 + \left(\frac{\sigma_{s^m} - \sigma_1}{s^m - 1} \right)^2}} \tag{22}$$

where $\Omega = \{2, 3, \cdots, s^m - 1\}$ denotes the set of singular value index; σ_k is the kth singular value; d_k represents the distance from k^{th} singular value to the line determined by points $(1, \sigma_1)$ and (s^m, σ_{s^m}); and $s^m = \lfloor s^{\max} \rfloor$ denotes the maximum integer less than $s^{\max}$. An example of the estimation procedure is shown in Fig. 6.
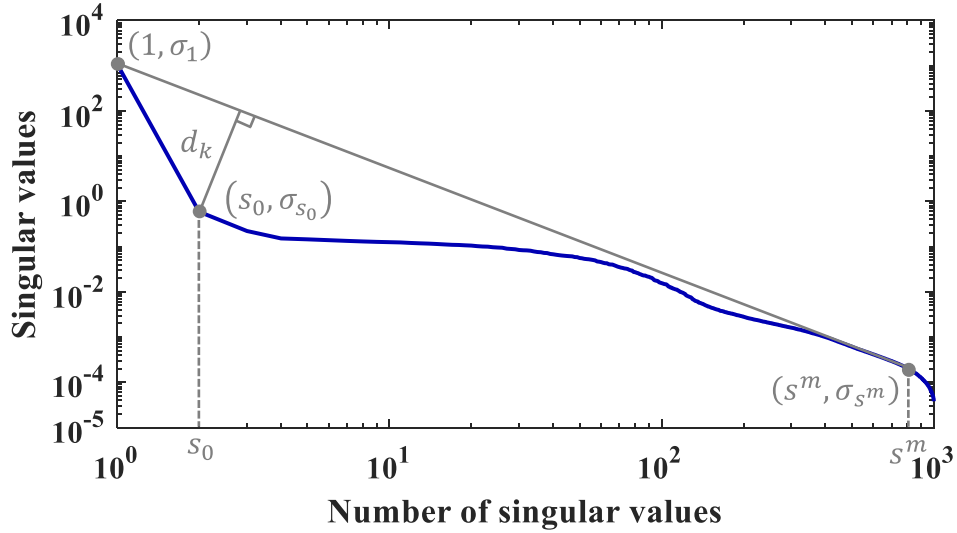

Fig. 6. Schematic for empirically determining the initial number of retained singular values.

4.2. Error requirement judgment based on EEB

Considering that advanced applications for the accuracy of PMU data, EEB is predefined, which denotes the lowest permitted accuracy for the applications. Since NMSE is a dimensionless scalar, and independent of measurement duration time T, NMSE is used for error judgment, as shown in Eq. (23).

$$\varepsilon_{\text{NMSE}}(i) \leq \varepsilon^{\text{Exp}} \tag{23}$$

When Eq. (23) holds for all the measurements $(i = 1, 2, \cdots, M)$, we consider that the expected error requirement is satisfied; otherwise, the expected error constraint is not satisfied.

4.3. Dynamic optimization of the number of retained singular values

When the accuracy does not meet the EEB, it is further judged whether s is greater than $s^{\max}$. When $s > s^{\max}$, the original data cannot accept any compression under the EEB, so the original PMU data without compression are transmitted directly; otherwise, s is self-increased by $s =$

$s + 1$ to ensure higher accuracy of the reconstructed data, and a new compression is performed. Then it is rechecked whether the new results meet the error requirement. On the contrary, when the accuracy meets EEB, s is self-decreased by $s = s - 1$, thereby improving the CR. To avoid the oscillation of s, a step of judgment is added to determine whether the optimal s has been obtained. If the value of s has appeared in the historical compression iterations, it indicates the optimal s is obtained, then the five sub-matrices $\overline{\boldsymbol{U}}_{11}^{s \times s}$, $\boldsymbol{U}_{21}^{(M-s) \times s}$, $\boldsymbol{\Sigma}_{11}^{\prime, s \times s}$, $\overline{\boldsymbol{V}}_{11}^{H, s \times s}$ and $\boldsymbol{V}_{12}^{H, s \times (N-s)}$ corresponding to the optimal s are finally transmitted.

5. Case studies and analysis

5.1. Test data of the PMU measurements

The proposed improved compression method has been implemented based on real measured data of 13 PMUs from a pilot project in China. The PMU data used in this paper are time tagged data with the sampling frequency of 50Hz and the corresponding sampling interval of 20ms. Data types of PMU measurements include three-phase nodal voltages (including amplitude $U^{(A)}$ and phase angle $U^{(P)}$), three-phase branch currents (including amplitude $I^{(A)}$ and phase angle $I^{(P)}$), three-phase total active power P, three-phase total reactive power Q, and system frequency f. The measurement data for 10 minutes starting at 10:00 am on July 18, 2019 are selected for the test, which corresponds to 30000 data points for each data type. Three-phase nodal voltages or branch currents are considered to be the same data type.

Seven measurement data matrices are constructed and normalized, corresponding to node voltage amplitude/phase angle, branch current amplitude/phase angle, three-phase total active power, three-phase total reactive power, frequency. Since the voltage and current data are three-phase signals, these three-phase signals are built in the same matrix with the dimension of 39×30000, whereas the dimensions of other matrices are 13×30000. The horizontal and vertical dimensions of the measurement data matrices are extremely unbalanced, which may affect

the efficiency of SVD [34]. To reduce the time cost of SVD, the matrices are sequentially rear-ranged into 1170×1000 and 390×1000, respectively. Namely, the original 30000 data per row are split into multiple segments, each segment contains 1000 data; finally, these segments are arranged from top to bottom to form a new matrix.

The voltage level of the actual pilot project is 10kV, and the system frequency is 50Hz, as well as the total active load is 50MW. Thus, the base values of three-phase total active and reactive power are set as 50MW and 50Mvar, respectively. The base values of voltage and current are set as phase voltage and phase current values. The base values for different data types are given in Table 1.

<p style="text-align:center;">**Table 1** Base values for different data types.</p>

Data types	$U^{(A)}$ (kV)	$U^{(P)}$ (rad)	$I^{(A)}$ (A)	$I^{(P)}$ (rad)	P (MW)	Q (Mvar)	f (Hz)
Base values	6.0	3.14	1500	3.14	50	50	50

To verify the proposed dynamic optimization strategy in Section 4, two groups of EEBs are predefined: Error I and Error II, as shown in Table 2. These EEBs can adequately satisfy the typical applications in distribution networks such as state estimation, energy management and optimal voltage control, and can be easily adjusted in different applications and periods.

<p style="text-align:center;">**Table 2** EEBs for different data types.</p>

Error groups	$U^{(A)}$	$U^{(P)}$	$I^{(A)}$	$I^{(P)}$	P	Q	f
Error I	1.0E-8	1.0E-6	1.0E-5	1.0E-6	1.0E-5	1.0E-5	1.0E-10
Error II	1.0E-7	1.0E-5	1.0E-4	1.0E-5	1.0E-4	1.0E-4	1.0E-9

The proposed method is tested utilizing MATLAB R2018b on a computer with an Intel(R) Xeon(R) CPU E5-2603 v3 @1.60GHz processor and 8GB RAM.

5.2. Accuracy analysis of the reconstructed data

Three types of measured data from PMU#1 are adopted to show the fidelity of the reconstructed data, including phase-A voltage amplitude $U_A^{(A)}$, phase-A current phase angle $I_A^{(P)}$, and three-phase total active power P, as illustrated from Figs. 7 to 9. The blue solid curve denotes the original PMU data, while the red dotted curve and green dot-dash curve denote the reconstructed data under Error I and Error II, respectively. It can be seen that the reconstructed data coincide the original data well. Thus, the data could be compressed with high accuracy. Also, the accuracy of reconstructed data under Error I is obviously higher than that under Error II, which also confirms that the smaller the EEB is predefined, the higher the accuracy of the data can be obtained after decompression. But this comes at the expense of reducing the compression performance.
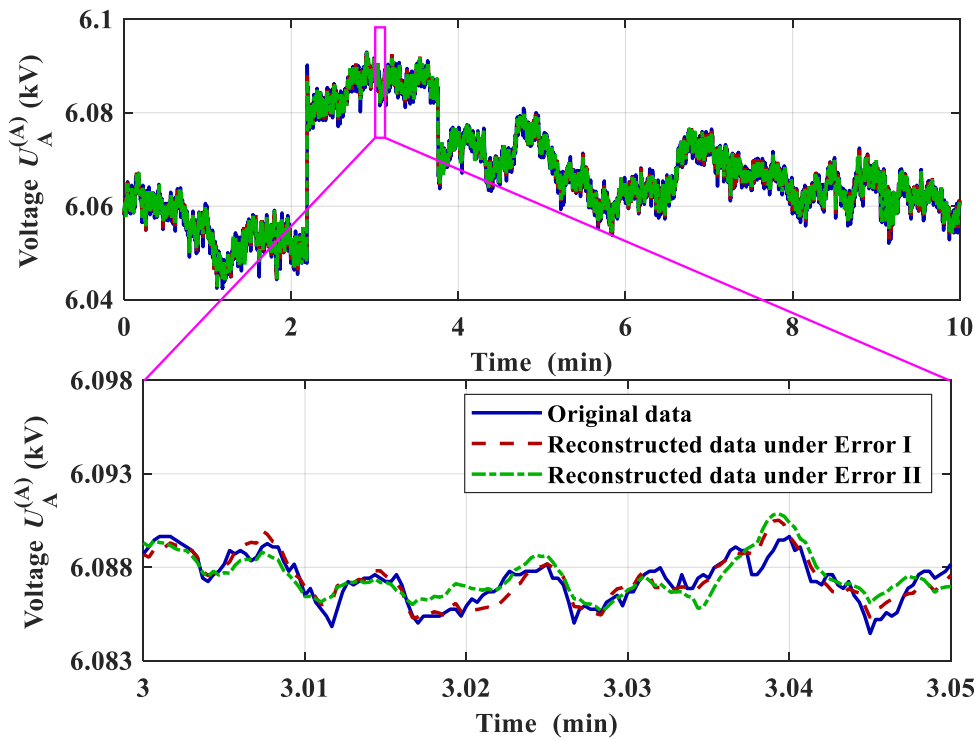

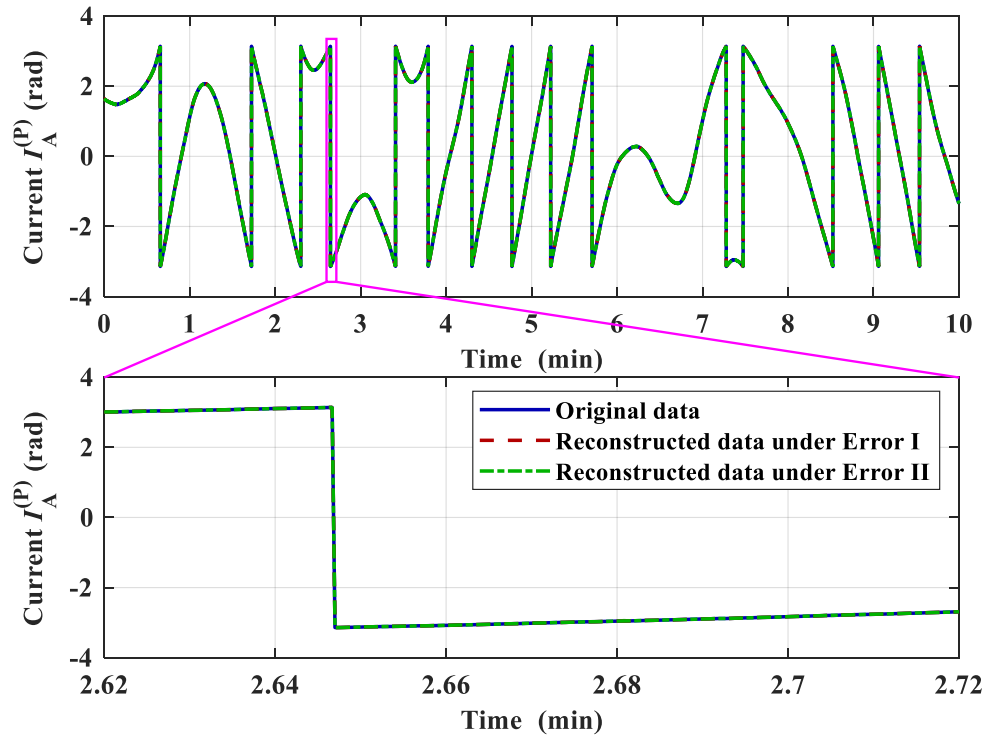**Fig. 7.** Phase-A voltage amplitude profile under Error I and Error II.

20

Fig. 8. Phase-A current phase angle profile under Error I and Error II.
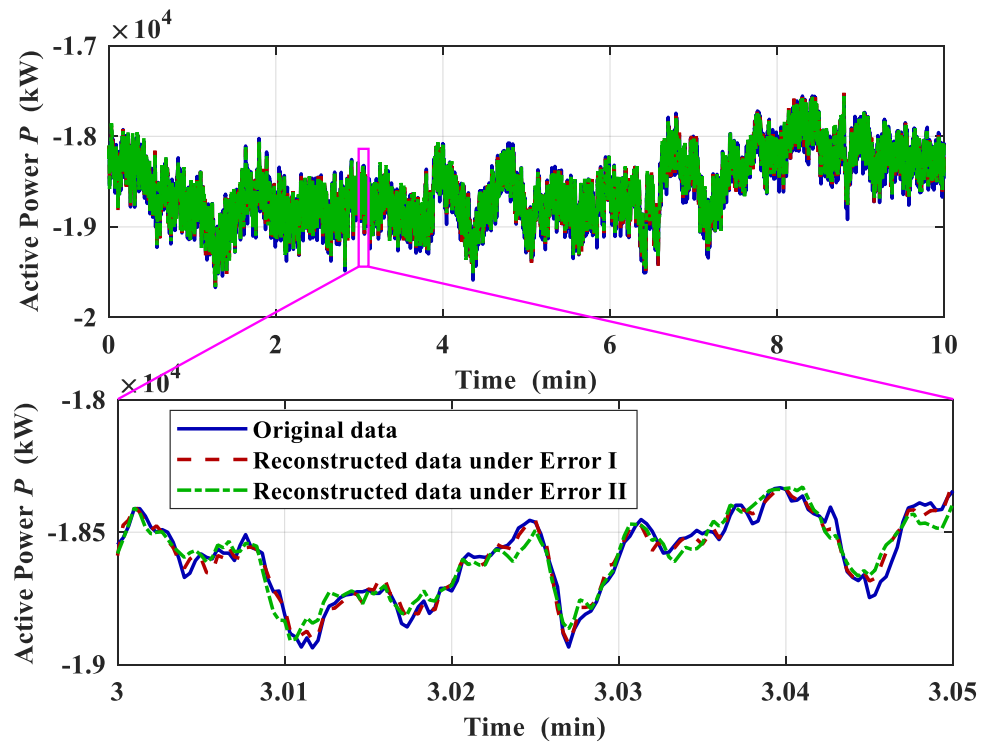

Fig. 9. Three-phase total active power profile under Error I and Error II.

5.3. Comparison with other data compression method

A comparison of the traditional SVD-based method, the proposed improved SVD-based method, and exception compression with swing door trending compression (ESDC) method [30] is shown in Table 3. The gain percentage refers to the improvement of the proposed method compared to the traditional SVD-based method.

Table 3 Compression of ESDC, traditional SVD-based and improved SVD-based method.

	Method	$U^{(A)}$ (kV)	$U^{(P)}$ (rad)	$I^{(A)}$ (A)	$I^{(P)}$ (rad)	P (MW)	Q (Mvar)	f (Hz)
CRs	ESDC	9.981	9.981	1.776	1.776	1.666	1.488	9.996
	Traditional SVD-based method	8.692	2.778	12.832	1.393	4.248	3.048	18.692
	Improved SVD-based method	8.943	134.917	13.079	11.476	4.456	3.261	18.882
	Gain percentage (%)	2.899	4756	1.920	723.800	4.896	7.000	1.017
MAEs	ESDC	0.006	5.654	1.172	4.903	18.879	0.007	0.009
	Traditional SVD-based method	0.009	0.021	1.493	0.099	19.530	0.004	0.003
	Improved SVD-based method	0.009	0.024	1.493	0.038	19.530	0.004	0.003

It can be seen that the improved SVD-based method has higher CRs for all data types than the traditional SVD-based method and the same reconstruction errors. It is the benefit of further compression of sub-matrices $\overline{U}_{11}$ and $\overline{V}_{11}^{H}$. In addition, when the CR obtained by the traditional method is smaller, the gain percentage achieved by the improved method is larger. A relatively larger number of retained singular values means that the sub-matrices $\overline{U}_{11}$ and $\overline{V}_{11}^{H}$ are further losslessly compressed with a larger amount of data.

Compared with ESDC, the improved SVD-based method shows better performance on the compression ratio and accuracy of the phase angle data. It is mainly the benefit from the lossless phase angle conversion. The performance of our method is basically at the same level with ESDC in terms of voltage amplitude, and surpasses it in rapidly fluctuating data such as current, active power, reactive power, and frequency. This is because the method can consider a longer time window and eliminate the effect of fluctuations.

5.4. Improvement of compression performance by phase angle conversion

The compression performance before and after performing phase angle conversion is compared to verify its benefits. The results in Table 4 show that the CR is limited if the original discontinuous phase angle data is directly compressed. After performing the phase angle conversion, the CRs of voltage and current phase angle data can be improved by more than 40 times and 5 times, while maintaining high accuracy. It can also be seen that voltage phase angle has higher CRs than current phase angle. This is mainly because the voltage is usually maintained at a relatively stable level, while the current may vary with the different types, sizes, and locations of loads.

Table 4 Comparisons of CRs and MAEs before and after performing phase angle conversion.

	CRs		MAEs	
Data types	$U^{(P)}$	$I^{(P)}$	$U^{(P)}$ (rad)	$I^{(P)}$ (rad)
Before phase angle conversion	3.049	1.694	0.021	0.010
After phase angle conversion	134.917	11.476	0.024	0.038
Gain percentage (%)	4325.000	577.450	/	/

5.5. Compression in the steady and dynamic states

An event of three-phase short-circuit fault recorded by PMUs is adopted to verify the compression performance of the proposed method in dynamic states. The phase angle data in the recorded data is shown in Fig. 10, and the fault lasts for 3.803 minutes. One of the steady-state measurements is replaced by the recorded three-phase fault data, and the compression is performed in the same way as the steady-state.
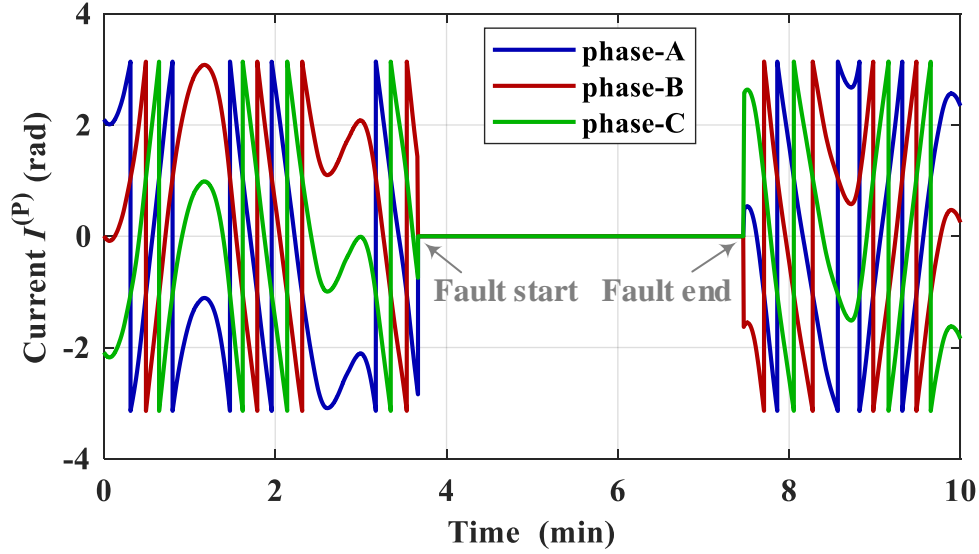
Fig. 10. Recorded current phase angle in the three-phase fault state.

Table 5 lists the CRs and NMSEs for different data types under steady and fault conditions, respectively. It is shown that the CRs in dynamic state are slightly lower than that of steady-state data. Meanwhile, both the steady and dynamic states' errors can be strictly controlled within the predefined expected error bounds (EEBs). Phase-A fault current phase angle is adopted to show the fidelity of the reconstructed data, as illustrated from Fig. 11. The blue solid curve denotes the original data, while the green dot-dash curve denotes the reconstructed data. It can be seen that the compressed PMU data could be reconstructed with high accuracy in dynamic state. These results indicate that the proposed method can effectively compress the PMU data during both steady and dynamic states.

Table 5 Comparison of compression performance between steady state and dynamic state.

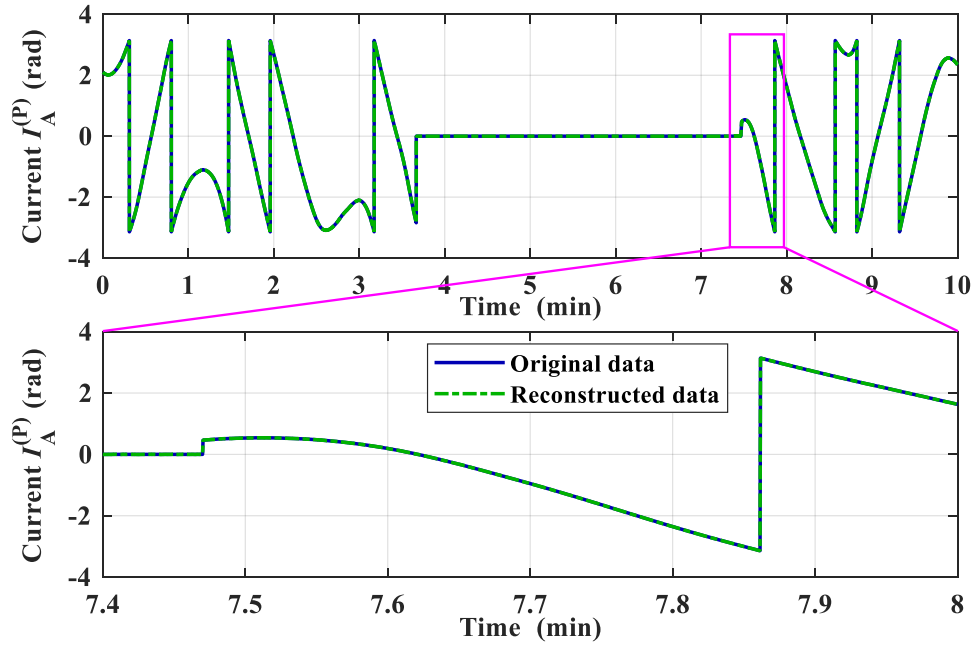| States		$U^{(A)}$	$U^{(P)}$	$I^{(A)}$	$I^{(P)}$	P	Q	f
Steady	CRs	8.943	134.917	13.079	11.476	4.456	3.261	18.882
	NMSEs	9.90E-8	3.52E-6	9.93E-5	9.96E-6	9.83E-5	9.96E-5	9.99E-10
Dynamic	CRs	8.806	107.983	12.780	11.247	4.456	3.294	17.714
	NMSEs	9.31E-8	7.52E-6	9.69E-5	9.75E-6	9.85E-5	9.87E-5	9.38E-10

Fig. 11. Phase-A fault current phase angle profile.

5.6. Verification of the proposed dynamic optimization strategy
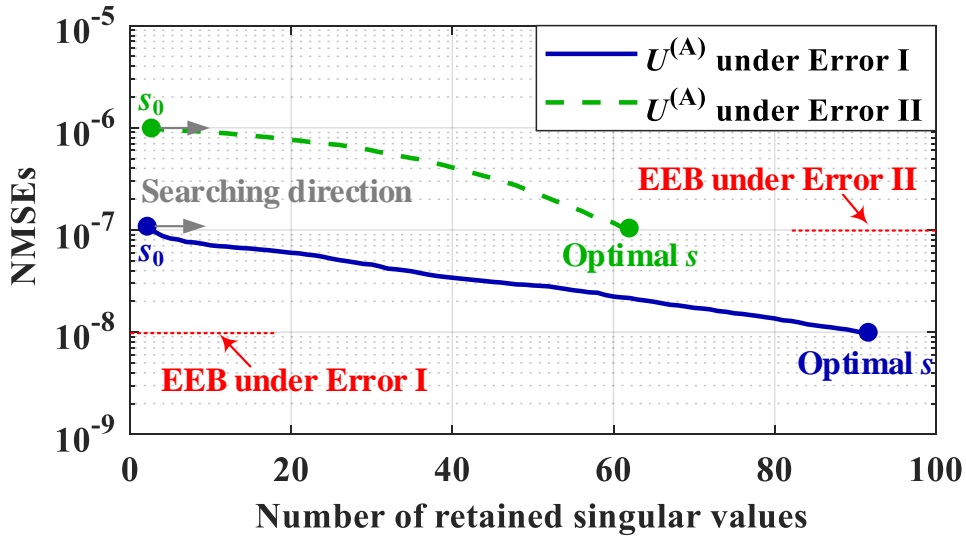
The numbers of retained singular values under Error I and Error II are listed in Table 6. It can be seen that the numbers of retained singular values under Error II are less than that under Error I, which indicates that less PMU data needs to be transmitted to DMS under Error II.

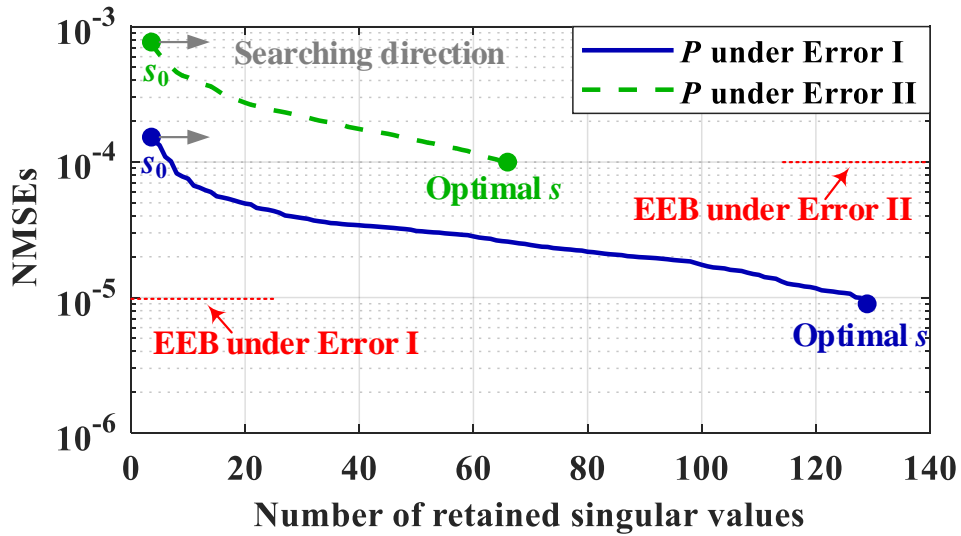**Table 6** The numbers of retained singular values for different data types.

Error groups	$U^{(A)}$	$U^{(P)}$	$I^{(A)}$	$I^{(P)}$	P	Q	f
Error I	91	8	198	150	128	190	103
Error II	62	5	42	48	66	92	15

Two types of data are selected to demonstrate the dynamic optimization processes of the number of retained singular values under the predefined error control bound, including the voltage amplitude $U^{(A)}$ and three-phase total active power P, as presented in Fig. 12. It can be seen that NMSEs corresponding to the initial number of retained singular values are larger than the predefined EEBs. The optimization process increases the number of retained singular values; consequently, NMSEs gradually decrease and approach the predefined EEBs. Also, the largest

NMSEs are less than the EEBs, indicating that the proposed optimization strategy is feasible and effective.

(a) Voltage amplitude

(b) Three-phase total active power

Fig. 12. Largest NMSEs with different numbers of retained singular values.

The execution time of different stages are presented in Table 7. It is shown that the maximum compression time is 0.848s. The lossless compression takes almost no extra time, because the reserved data is directly extracted from sub-matrices. However, it takes time to recover the com-

pressed elements in sub-matrices by solving a set of linear equations. The average extra decompression time due to the lossless compression is around 0.3s. The data decompression is carried out in DMS, so it will not bring much computing time and delay. As the time scale of distribution network applications varies from ten seconds to minutes, it can meet the demand of PMU applications. The overall time cost may be increased because of the searching process of the optimal compression scale with the given error bound. However, the increase is also limited in real applications due to the proper estimation of initial number of retained singular values, and the inheritance mechanism of singular value number in the searching iterations.

Table 7 The execution time for the compression of different data types.

Data types	Compression time	Decompression time		Total execution time
		Lossless	Lossy	
$U^{(A)}$	0.761s	0.218s	0.121s	1.100s
$U^{(P)}$	0.848s	0.123s	0.273s	1.244s
$I^{(A)}$	0.838s	0.153s	0.130s	1.121s
$I^{(P)}$	0.759s	0.809s	0.623s	2.191s
P	0.139s	0.154s	0.045s	0.338s
Q	0.155s	0.325s	0.100s	0.580s
f	0.132s	0.089s	0.036s	0.257s

6. Conclusion

High sampling rates in PMUs generate huge volumes of measurement data, which cause heavy data transmission burdens for communication systems. In this paper, an improved SVD-based method for PMUs measurement data in distribution networks is proposed. First, for the original discontinuous phase angle, a lossless phase angle conversion method is proposed, which converts the discontinuous phase angle data of PMU into continuous data sequence to enhance CR. Then, a PMU data compression method is proposed based on SVD, and the compression capability is further enhanced by a lossless compression that utilizes the orthogonal property of the two sub-matrices generated by SVD. Moreover, an error control strategy is designed to dynamically

optimizes the scale of transmitted data according to the accuracy requirement of different applications in distribution networks. Case studies are performed on real PMUs measurement data to show the compression performance and the reconstructed data accuracy. Results show that, due to the benefit of the phase angle conversion and the ignoring of some low-value singular values, the amount of data transmitted throughout communication networks can be significantly reduced. Also, the CRs of the proposed method are better than the traditional SVD methods given the same reconstruction errors. Besides, the proposed method will effectively compress the PMU data during both the steady and dynamic states. For the future work, it can consider to combine the proposed method with real-time compression technology used at PMU locations to achieve better compression performance.

CRediT authorship contribution statement

Jinli Zhao: Conceptualization, Methodology. **Yuzhuan Ye:** Data curation, Writing - original draft. **Hao Yu:** Supervision, Writing - review & editing. **Peng Li:** Investigation, Software. **Peng Li:** Software, Formal analysis. **Jianzhong Wu:** Validation. **Chengshan Wang:** Project administration.

Declaration of Competing Interest

The authors declare that they have no known competing financial interests or personal relationships that could have appeared to influence the work reported in this paper.

Appendix A

The increment $\delta_{i,j}$ is a non-negative integer multiple of 2π, thus $\delta_{i,j} = 2m\pi$ $(m \in \{0,1,2,\cdots\})$.

1) Suppose $x_{i,j} < x_{i,j-1}^{con}$, then $x_{i,j}^{con}$ is presented as follows:

$$x_{i,j}^{con} = x_{i,j} + \delta_{i,j} = x_{i,j} + 2m\pi \tag{A.1}$$

If $m = 0$, the phase angle $x_{i,j}$ has not been converted. Then we have

$$x_{i,j}^{rec} = x_{i,j}^{con} = x_{i,j} \tag{A.2}$$

If $m \geq 1$ ($m \in \{1,2,3,\cdots\}$), we have $x_{i,j}^{con} \geq \pi$. In this case, if $x_{i,j}^{con} = k\pi$ ($k \in \{1,3,5,\cdots\}$), then

$k = 2m - 1$, and $x_{i,j}^{rec}$ can be calculated by Eq. (A.3).

$$
\begin{aligned}
x_{i,j}^{rec} &= x_{i,j}^{con} - \delta_{i,j}' \\
&= x_{i,j} + 2m\pi - (k+1) \times \pi \\
&= x_{i,j}
\end{aligned}
\tag{A.3}
$$

If $x_{i,j}^{con} > \pi$ and $x_{i,j}^{con} \neq k\pi$, the $x_{i,j}^{rec}$ can be calculated by Eq. (A.4).

$$
\begin{aligned}
x_{i,j}^{rec} &= x_{i,j}^{con} - \delta_{i,j}'' \\
&= x_{i,j} + 2m\pi - \left\lceil \frac{x_{i,j} + 2m\pi - \pi}{2\pi} \right\rceil \times 2\pi \\
&= x_{i,j} - \left\lceil \frac{x_{i,j} - \pi}{2\pi} \right\rceil \times 2\pi
\end{aligned}
\tag{A.4}
$$

Since $x_{i,j}^{con} \neq k\pi$, then $x_{i,j} \in (-\pi, \pi)$. We have $\left\lceil \frac{x_{i,j}-\pi}{2\pi} \right\rceil \times 2\pi = 0$, thus $x_{i,j}^{rec} = x_{i,j}$. The analysis

shows that the phase angle can be restored losslessly in the case of $x_{i,j} < x_{i,j-1}^{con}$.

2) Suppose that $x_{i,j} \geq x_{i,j-1}^{con}$, then $x_{i,j}^{con}$ is presented as follows:

$$x_{i,j}^{con} = x_{i,j} - \delta_{i,j} = x_{i,j} - 2m\pi \tag{A.5}$$

If $m = 0$, the phase angle $x_{i,j}$ has not been converted. Then we have

$$x_{i,j}^{rec} = x_{i,j}^{con} = x_{i,j} \tag{A.6}$$

If $m \geq 1$ ($m \in \{1,2,3,\cdots\}$), we have $x_{i,j}^{con} < -\pi$. In this case, the $x_{i,j}^{rec}$ can be calculated by Eq.

(A.7).

$$x_{i,j}^{\text{rec}} = x_{i,j}^{\text{con}} + \delta_{i,j}'''$$

$$= x_{i,j} - 2m\pi + \left\lceil \frac{-\left(x_{i,j} - 2m\pi + \pi\right)}{2\pi} \right\rceil \times 2\pi \qquad \text{(A.7)}$$

$$= x_{i,j} + \left\lceil \frac{-\left(x_{i,j} + \pi\right)}{2\pi} \right\rceil \times 2\pi$$

Since $x_{i,j} \in [-\pi, \pi)$, we have $\left\lceil \frac{-(x_{i,j}+\pi)}{2\pi} \right\rceil \times 2\pi = 0$, thus $x_{i,j}^{\text{rec}} = x_{i,j}$. The analysis shows that the

phase angle can be restored losslessly in the case of $x_{i,j} \geq x_{i,j-1}^{\text{con}}$.

References

[1] Zhang Y, Xu Y, Yang H, et al. Voltage regulation-oriented co-planning of distributed generation and battery storage in active distribution networks. Int J Electr Power Energy Syst 2019;105:79-88.

[2] Hassanzadehfard H, Jalilian A. Optimal sizing and location of renewable energy based DG units in distribution systems considering load growth. Int J Electr Power Energy Syst 2018;1:356-370.

[3] Ehsan A, Cheng M, Yang Q. Scenario-based planning of active distribution systems under uncertainties of renewable generation and electricity demand. CSEE J Power Energy Syst 2019;5(1):56-62.

[4] Li R, Zhao Z, Zhou X, et al. Intelligent 5G: when cellular networks meet artificial intelligence. IEEE Wireless Commun 2017;24(5):175-183.

[5] Su H, Wang C, Li P, et al. Optimal placement of phasor measurement unit in distribution networks considering the changes in topology. Appl Energy 2019;250(15):313-322.

[6] Ketabi A, Nosratabadi S, Sheibani M. Optimal PMU placement with uncertainty using Pareto method. Math Prob Eng;2012:1-14.

[7] Nosratabadi S, Modarresi J. Phasor measurement units placement considering double contingency by differential evolution algorithm based on pareto method. IEEE Smart Grid Conference (SGC) 2017:1-6.

[8] Fiaschetti L, Antunez M, Trapani E, et al. Monitoring and controlling energy distribution: Implementation of a distribution management system based on common information model. Int J Electr Power Energy Syst 2018;94:67-76.

[9] Paternina M, Zamora-Mendez A, José A, et al. Model-based synchrophasor estimation by exploiting the eigensystem realization approach. Electr Power Syst Res 2020;182:1-12.

[10] Mccamish B, Kulkarni J, Ke Z, et al. A rapid PMU-based load composition and PMU estimation method. Electr Power Syst Res 2017;143:44-52.

[11] Zhao Z, Yu H, Li P, et al. Optimal placement of PMUs and communication links for distributed state estimation in distribution networks. Appl Energy 2019;256:113963.

[12] Al-Jaafreh M and Mokryani G. Planning and operation of LV distribution networks: a comprehensive review. IET Energy Syst Integr 2019;1(3):133-146.

[13] Ebrahim M, Wadie F, Abd-Allah M. Integrated fault detection algorithm for transmission, distribution, and microgrid networks. IET Energy Syst Integr 2019;1(2):104-113.

[14] Guo Y, Wu W, Zhang B, et al. A distributed state estimation method for power systems incorporating linear and nonlinear models. Int J Electr Power Energy Syst 2015;4:608-616.

[15] Pegoraro P, Meloni A, Atzori L, et al. PMU-based distribution system state estimation with adaptive accuracy exploiting local decision metrics and IoT paradigm. IEEE Trans Instrum Meas 2017;6(4):704-714.

[16] Li P, Ji H, Yu H, et al. Combined decentralized and local voltage control strategy of soft open points in active distribution networks. Appl Energy 2019;241(3):613-624.

[17] Sadeghian O, Nazari-Heris M, Abapour M, et al. Improving reliability of distribution networks using plug-in electric vehicles and demand response. J Mod Power Syst Clean Energy 2019;7(5):1189-1199.

[18] Orozco-Henao C, Bretas A, Herrera-Orozco A, et al. Towards active distribution networks fault location: contributions considering DER analytical models and local measurements. Int J Electr Power Energy Syst 2018;99:454-464.

[19] Zhang T, Yuan P, Du Y et al. Robust distributed state estimation of active distribution networks considering communication failures. Int J Electr Power Energy Syst 2020;118:105732.

[20] Tsitsimelis A, Antón-Haro C. A regularized state estimation scheme for a robust monitoring of the distribution grid. Int J Electr Power Energy Syst 2020;117:105621.

[21] Chai W, Wang N, Katsaros K, et al. An information-centric communication infrastructure for real-time state estimation of active distribution networks. IEEE Trans Smart Grid 2015;6(4):2134-2146.

[22] Li P, Ji H, Wang C, et al. Coordinated control method of voltage and reactive power for active distribution networks based on soft open point. IEEE Trans Sustain Energy 2017;8(4):1430-1442.

[23] Tcheou M, Lovisolo L, Ribeiro M, et al. The compression of electric signal waveforms for smart grids: state of the art and future trends. IEEE Trans Smart Grid 2013;5(1):291-302.

[24] Wen L, Zhou K, Yang S, et al. Compression of smart meter big data: a survey. Renew Sustain Energy Rev 2018;9-69.

[25] Littler T, Morrow D. Wavelets for the analysis and compression of power system disturbances. IEEE Trans Power Del 1999;4(2):358-364.

[26] Liu S, Zhao Y, Lin Z, et al. Data-driven event detection of power systems based on unequal-interval reduction of PMU data and local outlier factor. IEEE Trans Smart Grid 2020;1(2):1630-1643.

[27] De S, Assis T, Pal, et al. Data compression in smart distribution systems via singular value decomposition. IEEE Trans Smart Grid 2017;8(1):275-284.

[28] Das S, Singh S. Application of compressive sampling in synchrophasor data communication in WAMS. IEEE Trans Ind Inf 2014;10(1):450-460.

[29] Gadde P, Biswal M, Brahma S, et al. Efficient compression of PMU data in WAMS. IEEE Trans Smart Grid 2016;7(5):2406-2413.

[30] Zhang F, Cheng L, Li X, et al. Application of a real-time data compression and adapted protocol technique for WAMS. IEEE Trans Power Syst 2014;30(2):653-662.

[31] Hamid E, Kawasaki Z. Wavelet-based data compression of power system disturbances using the minimum description length criterion. IEEE Trans Power Del 2002;17(2):460-466.

[32] Ning J, Wang J, Gao W, et al. A wavelet-based data compression technique for smart grid. IEEE Trans Smart Grid 2010;2(1):212-218.

[33] IEEE standard for synchrophasor measurements for power systems. IEEE Std C37.118.1-2011;2011:1-61.

[34] Wu T, Sarmadi S, Venkatasubramanian V, et al. Fast SVD computations for synchrophasor algorithms. IEEE Trans Power Syst 2016;31(2):1651-1652.